Electrochimica Acta 253 (2017) 163–170

Contents lists available at ScienceDirect

Electrochimica Acta

journal homepage: www.elsevier.com/locate/electacta

Electrochemical Characterization of Lithium-Ion Battery Cathode Materials with Aqueous Flowing Dispersions

Zhaoxiang Qi, Hongxu Dong, Gary M. Koenig Jr.*

Department of Chemical Engineering, University of Virginia, 102 Engineers Way, Charlottesville, VA, 22904-4741, USA

ARTICLE INFO

Article history:
Received 8 August 2017
Received in revised form 4 September 2017
Accepted 5 September 2017
Available online 6 September 2017

Keywords:
Battery Material Characterization
Flowing Particle Analysis
Lithium-Ion Battery
Dispersed Particle Resistance
Particle Suspension

ABSTRACT

Battery active materials are evaluated using numerous material characterization techniques for fundamental understanding, comparative analysis during research and development, and for quality control during manufacturing. Electrochemical properties of the active materials also need to be investigated and validated, and this analysis is very time and material intensive generally requiring electrode fabrication, cell assembly and cell cycling. In addition, evaluating active materials electrochemically in battery cells can be complicated by the electrode microstructure and the contributions of other components within the cell that are not the active materials. In this report, an active material characterization method is demonstrated to provide electrochemical insights for lithium-ion cathode materials by dispersing them into aqueous electrolyte and flowing through an electrochemical reaction cell. This method requires very little active material and time to conduct the measurements, typically requiring under 0.1 grams of material and less than 10 minutes. The measured resistance from this technique provides insights into the electrochemical performance of the active material and generally correlates to the rate capability. This measured resistance is insensitive to other electrode components or electrode microstructure because there is no electrode fabrication step. $LiFePO_4$ was chosen as a commercial material for initial demonstration of the technique.

1. Introduction

Lithium iron phosphate ($LiFePO_4$, LFP) is an attractive lithium-ion cathode active material due to its high capacity, cycling stability, and abundancy of raw materials used in its production [1–4]. However, the conductivity of LFP is low relative to other cathode material candidates; therefore, extensive research has been done to improve the high power performance of LFP by controlling the particle morphology, coating with conductive carbon, and doping with other elements [1,5–14]. Although notable improvements have been achieved, LFP electrochemical performance varies significantly across different methods and between different batches from the same method [1,5–16]. In addition, LFP material researchers synthesize significant numbers of variations of LFP materials during optimization through modification of synthesis parameters. These materials all need to be characterized to understand the electrochemical performance and perform comparative analysis. While characterization of LFP materials is necessary during research and development, LFP manufacturers also need to test LFP final products before shipping to electrode and cell manufacturers. The conventional method to test electrode materials involves electrode fabrication, cell assembly, and battery cycling [5,17–19]. Although valuable for material comparison and/or validation, electrochemical cell testing requires extensive effort, materials, and time. In addition, battery cycling performance results can be ambiguous because the measured performance reflects not only the LFP material properties but also the material properties of the other cell components, multiple material interfaces, the electrode microstructure, and heterogeneity of materials throughout the electrodes and cell. For example, the properties and distribution of carbon and binder additives directly impact the cell electrochemical performance [20–22], and even the pressure applied to the electrode can influence the resulting cell resistance [23]. These variations are very challenging to control and to independently characterize and identify.

Our research group previously reported a characterization method we refer to as “Dispersed Particle Resistance” (DPR) and applied the technique to characterize $Li_4Ti_5O_{12}$ (LTO) anode materials dispersed in organic electrolytes [24]. DPR involved a series of chronopotentiometry or chronoamperometry steps on active material suspensions. This series of measurements resulted in a number of currents measured for successively varied

* Corresponding author.
E-mail address: gary.koenig@virginia.edu (G.M. Koenig).

http://dx.doi.org/10.1016/j.electacta.2017.09.031
0013-4686/

potentials or potentials measured for successively varied currents, and in either case the slope from a linear fit of the potential-current relationship from these battery active material dispersions resulted in a resistance – the DPR of the suspension. This resistance was measured during the collision and electrochemical reactions of battery active material particles with an electrode, and the primary contribution to the resistance resulted from the particles themselves. The previous study demonstrated a correlation between DPR and the rate capability of the LTO active materials in identically prepared coin cells. The DPR method was demonstrated to be relatively fast (< 30 minutes), and could be operated in succession for different material batches or different particle loadings; however, the technique was still a batch-wise process which hindered continuous operation and high throughput [24]. Another challenge with the initial demonstration of the technique was the use of organic lithium-ion battery electrolyte as the dispersion fluid, resulting in the need to isolate the entire system from ambient atmospheric conditions and requiring flammable and relatively expensive solvents and salts. The use of lithium metal as the counter electrode also contributed to additional safety concerns [25,26].

Herein, we report major advances to the DPR characterization method, and apply the new procedures to characterize lithium-ion cathode materials in aqueous electrolyte in a continuous mode of operation. LFP was chosen as the first active material to demonstrate this analysis because 1) LFP has a flat charge/discharge plateau which improves the consistency of DPR analysis, 2) the electrochemical potential of LFP intercalation/deintercalation allows the use of aqueous carrier fluids for the suspension, and 3) LFP is stable in aqueous electrolyte, in particular within the short measurement time of the DPR technique [24,27–30]. A new custom electrochemical flow cell was designed for continuous analysis and successfully decreased the total operation time to < 10 minutes. LFP was suspended in aqueous electrolyte, providing operating convenience and improved safety relative to organic electrolytes [24,31,32]. Six different LFP materials were characterized using the DPR technique in a flow-through cell to provide confidence in the new method for the characterization of electrode active materials and the correlation between rate capability and DPR with the new electrolyte and cell design. The ability of the DPR technique to detect aging effects of LFP exposed to aqueous electrolyte also was demonstrated.

2. Experimental

2.1. Material Synthesis and Characterization

Six different LFP materials were characterized, which we refer to as LFP-1, LFP-2, LFP-3, LFP-4, LFP-5, and LFP-6. These materials were purchased from different suppliers and used as received. Scanning electron microscope (SEM) images were taken for all LFP materials with a Quanta 650 SEM to characterize the morphologies of the powders. A Panalytical X'pert diffractometer with Cu Kα radiation was used to obtain the X-ray diffraction (XRD) patterns of the materials between 2θ values of 15 and 65 degrees. Tap densities were measured with a tap density analyzer with sample volumes typically ~6 mL in a 10-mL graduated cylinder (Quantachrome Instruments). Thermogravimetric analysis (TGA) of the LFP samples in air was conducted with a TA Instruments Q50. TGA was performed at a ramp rate of 5 °C min^{-1} from room temperature to 800 °C. BET surface area of the LFP materials was determined with a surface area and pore size analyzer using nitrogen as the probe gas (NOVA 2200e). The Fe concentration of the electrolyte was measured using inductively coupled plasma optical emission spectroscopy (ICP) analysis (PerkinElmer Optima 8000). The typical concentration range for ICP analysis was 0.1 to 100 ppm for the element Fe. To prepare ICP samples, the electrolyte was carefully separated from the remaining solid LFP particles via filtration and then diluted to the desired concentration. The Fe concentration reported was the average of three separate measurements. The standard deviations of all ICP measurements were less than 1% of the reported average values.

2.2. Coin Cell Fabrication and Electrochemical Characterization

All LFP materials were characterized electrochemically first using conventionally fabricated coin cells. Electrochemical characterizations were carried out using CR2032-type coin cells with a LFP electrode as the working electrode and lithium foil as the counter and reference electrode, separated by a polypropylene/polyethylene/polypropylene trilayer membrane. LFP electrodes were prepared by first mixing 60 wt% LFP powder with 20 wt% carbon black and 20 wt% polyvinylidene difluoride (PVDF) binder, which was dissolved in *N*-methylpyrrolidone (NMP, Sigma-Aldrich®). Relatively high carbon content was used to ensure good connectivity and high conductivity between LFP particles and relatively high binder content was used to provide good mechanical robustness of the electrode films and adhesion to the current collector. For coin cells made to demonstrate the impact of excess carbon in the LFP samples, electrodes were also fabricated without any additional carbon black additive. These electrodes were comprised of 90 wt% LFP powder and 10 wt% PVDF binder. The mixtures were then pasted on an aluminum foil using a doctor blade with a gap thickness of 125 μm. Electrodes were dried in an oven at 70 °C overnight and further dried in a vacuum oven at 70 °C for an additional three hours while applying vacuum. Electrode disks of 1.6 cm^2 were prepared using a punch, and the loading of LFP active material in the electrodes for all samples was ~4 mg. The electrolyte for the coin cell measurements was 1.2 M lithium hexafluorophosphate ($LiPF_6$) in ethylene carbonate (EC) and ethyl methyl carbonate (EMC) with EC/EMC = 3:7 volume ratio (BASF Corporation). The cells were assembled in an argon-filled glove box (with concentrations of both O_2 and H_2O < 1 ppm) at room temperature. The galvanostatic charge-discharge cycling of coin cells were performed with a Maccor battery cycler. Where C rates are reported, they were determined by first measuring the gravimetric capacity of the LFP materials at 17 mA g^{-1}_{LFP} (measured capacities varied between 145 and 160 mAh g^{-1}_{LFP}). Then, the actual measured capacity at the low discharge rate was used for scaling C rates (e.g.; for measured 160 mAh g^{-1}_{LFP}, 0.1C was 16 mA g^{-1}_{LFP}, 1C was 160 mA g^{-1}_{LFP}, etc.). The cycling voltage window for LFP cells was 2.5 to 4.0 V (vs. Li/Li^+).

2.3. Active Material Suspensions Electrochemical Evaluation

The aqueous electrolyte used for LFP suspensions was 1 M Li_2SO_4 (Fisher Scientific) dissolved in distilled water. LFP suspensions were prepared by dispersing LFP powders into the aqueous electrolyte agitated by a magnetic stir bar at 500 rpm for 5 minutes before electrochemical measurements, consistently for all measurements. Different loadings of LFP suspensions (0.2 vol%, 0.4 vol%, 0.7 vol%, 1.0 vol%, 1.5 vol%, 2.0 vol%, 3.0 vol%, and 4.0 vol%) were also prepared to characterize the effect of loading on the measured resistance. A customized cell was designed and assembled to electrochemically characterize the suspensions (Fig. 1). As shown in Fig. 1, channels for both cathode and anode were carved using a scalpel (Fisher Scientific) and separated by a porous polypropylene membrane (25 μm thick, Celgard®). Both channel dimensions were 10 × 0.5 × 0.2 cm^3. The working electrode (cathode) was a gold wire (0.25 mm diameter and 30 cm length, Fisher Scientific). The counter electrode (anode) was a platinum wire (0.5 mm diameter and 8 cm length, Sigma Aldrich), and a Ag/AgCl electrode

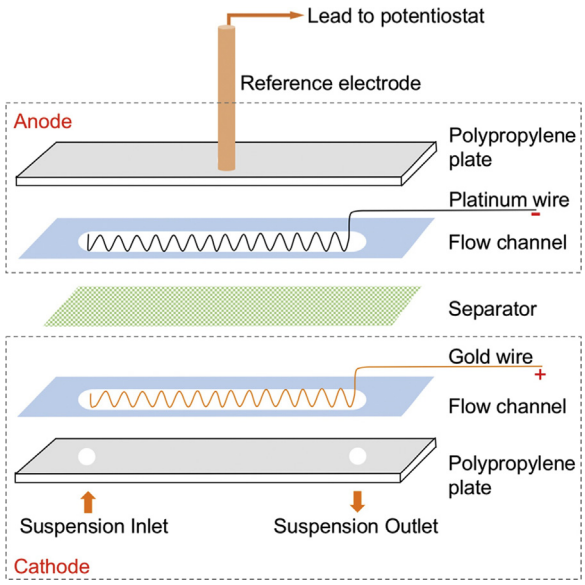

Fig. 1. Cartoon illustration of the custom electrochemical cell with gold wire as the working electrode in the channel, platinum wire as the counter electrode, and Ag/AgCl reference electrode.

(Pine Instruments) was used as the reference electrode. Flow of the suspensions was provided by a MasterFlex peristatic pump (Cole-Parmer) at a rate of 82 mL min^{-1}. All electrochemical tests, including chronoamperometry and electrochemical impedance spectroscopy (EIS), on this custom device were performed with a Biologic SP-150.

3. Results and Discussion

3.1. Electrochemical Testing with Conventional Coin Cells

The LFP materials were characterized using XRD, SEM, TGA, BET, and tap density first to confirm their material properties, and material characterization for the LFP materials can be found in the Supplementary Materials in Figs. S1, S2, and S3 and in Table S1. Conventional coin cells were then fabricated and cycled to evaluate electrochemical performance. The voltage profiles for the LFP materials at increasing rates of discharge (from 0.1C to 10C, all charge cycles were at 0.1C) are shown in Fig. 2. All LFPs had a flat discharge plateau at ~3.45 V at low rates, which was consistent with other reports on LFP materials [1,5–16,29]. Samples LFP-1 through LFP-5 had discharge capacities at low cycling rates that ranged from 145 to 160 mAh g^{-1}_{LFP}. These values were lower than the theoretical capacity of LFP (170 mAh g^{-1}_{LFP}), but within a similar range of other LFP material reports [1,5–16,29]. LFP-6 showed a significantly lower capacity even at the low rate of 0.1C. This was attributed to the high impurity content which resulted in multiple impurity peaks in the XRD pattern of this material (Fig. S1 in Supplementary Materials) [33,34]. Discharge voltages and capacities for all six LFP materials decreased with increasing rate. This is typical and consistent with the literature due to increasing overpotential at increasing discharge current [8–11,14,16,19,29,35–37]. However, the percentage of the capacity retention varied depending on the material. As shown in Fig. 3, LFP-1 showed the highest rate capability performance and LFP-6 the lowest. The capacity retention (in terms of the percentage of the discharge capacity relative to the capacity at 0.1C) at increasing rates, or rate capability, generally followed the order of LFP–1 > LFP–2 > LFP–3 > LFP–4 > LFP–5 > LFP-6. We note that LFP-4 showed slightly higher capacity retention than LFP-3 at 5C, although at this high current (~2 mA cm^{-2}) the lithium metal anode likely begins to impact the measurements [38,39]. These electrochemical measurements established the benchmark order of rate capability among the six LFP materials which were within identically processed composite electrodes. We note here that the focus of this manuscript is the DPR technique and the relationship between DPR measurements and coin cell electrochemical analysis, thus detailed characterization for diagnostics on the detailed differences in material and electrochemical properties between the LFP samples was not conducted.

3.2. LFP Suspension DPR Characterization

DPRs for LFP materials were measured using the following procedure. After dispersing a LFP powder in aqueous electrolyte, the suspension was electrochemically evaluated in a custom cell (shown in Fig. 1). A series of chronoamperometry tests at sequentially increasing potentials were performed for each suspension. Potentials were chosen such that the LFP particles were electrochemically oxidized/charged at each step. The potential and the average stabilized current for each step were retained for analysis. A plot of the potential vs. current resulted in a linear relationship for all electrochemical tests, and the slope of a linear fit of each data set was the DPR corresponding to a given material at a given loading (with loading referring to the vol% LFP in the electrolyte). An example of the linear potential vs. current data used to determine DPR, with 2 vol% LFP-3, is shown in Fig. 4. A new plateau at an increased current resulted for each step increase of potential in Fig. 4a. The average value of the current increased linearly with the increase in the applied potential. Fig. 4b shows the resulting data extracted from the experiment in Fig. 4a, with the applied potential vs. the average measured current of the last 10 seconds at that potential. For the example linear fit applied in Fig. 4b, the slope was 400.7 Ω (the DPR value) and $R^2 = 0.998$, indicating a good fit. The measured DPR was the sum of all of the contributions to the electrode overpotential and was thus a combination of several resistances, including the resistance of the active material particles which were in contact with the current collector, ohmic resistance of the external electrical connections, and the ohmic resistance from the electrolyte. The combination of the latter two resistances ranged between 1.5–2.5 Ω, as determined by the high frequency intercept of EIS measurements. The range of DPR values measured was between 38 and 1202 Ω, indicating that the resistance arising from the LFP particles undergoing electrochemical oxidation was the primary contributor to the measured DPR and that the linear response of the DPR technique was not simply due to the electrolyte resistance. We note that our initial report of the DPR technique had much more significant ohmic contributions ranging from 125 – 140 Ω [24]. The reduction of the ohmic contribution to the raw measured DPR resistance in this report was attributed to: 1) the significantly higher ionic conductivity of the aqueous electrolyte relative to the organic electrolyte (~100 mS cm^{-1} compared to ~15 mS cm^{-1}) [40]; 2) the change from an aluminum electrode in organic lithium-ion battery electrolyte to a gold electrode in aqueous electrolyte because the aluminum has a lower electronic conductivity and forms a passivation layer in the organic electrolyte that likely increased the measured resistance [41–44]. As discussed in a previous report, every contribution to DPR would be difficult to assess independently, but the dominant contribution was expected to be from the lesser of the ionic or electronic resistance from of the ensemble of active material particles colliding on the current collector and undergoing electrochemical reactions at any given time [24].

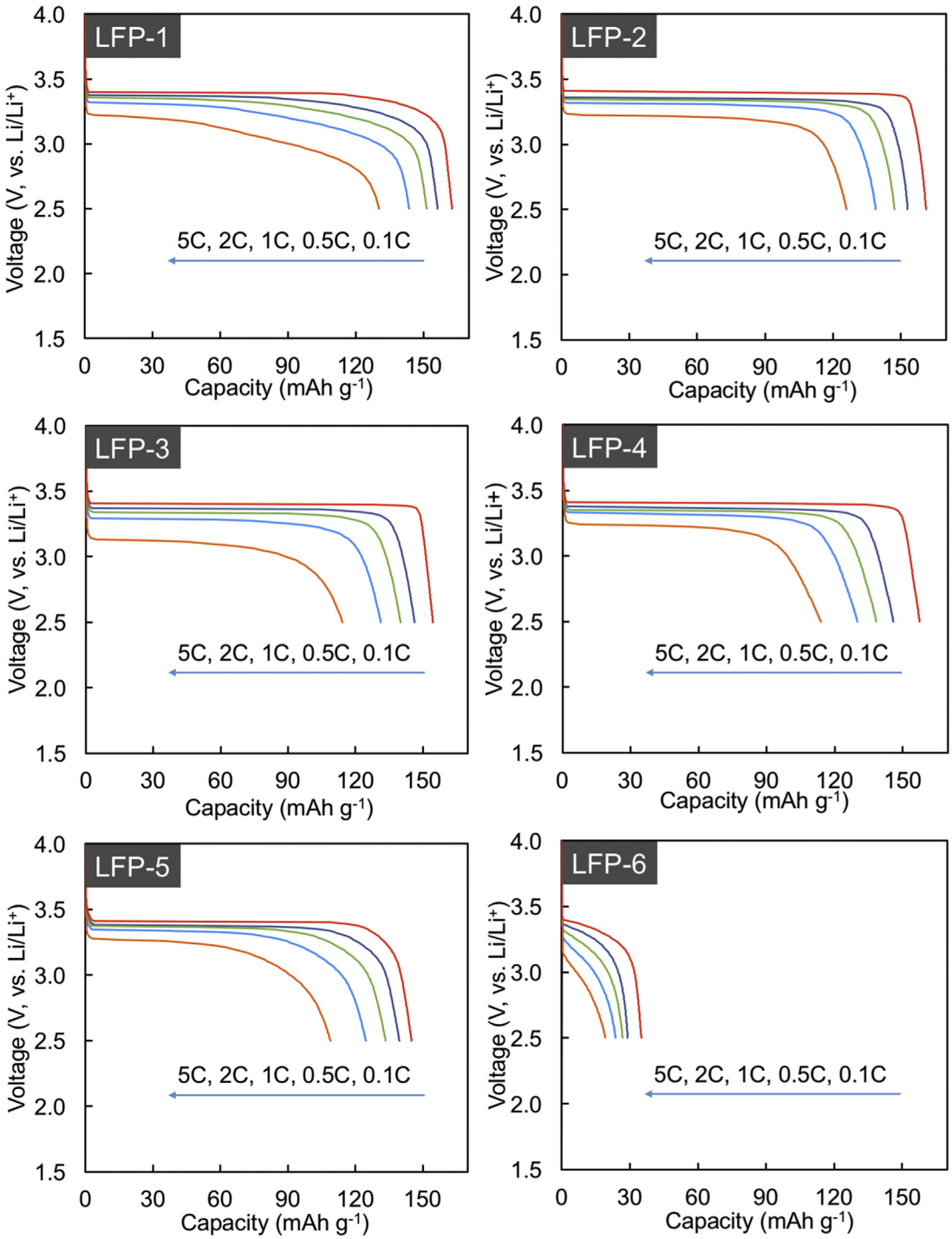

Fig. 2. Voltage profiles during constant current discharges at increasing C-rates for all six LFP materials. For all plots, the discharge curves correspond to 0.1C (red), 0.5C (dark blue), 1C (green), 2C (light blue), and 5C (orange). C rates were based on the gravimetric capacity of the material at 0.1C.

DPR values of a material can be influenced by a few key factors besides the intrinsic electrochemical properties of the active material, including the electrochemical cell design (cell size, wire length and geometry), suspension flow rate, and active material loading. The same cell was used for each series of measurements to exclude any cell variability, and the flow rate was also kept constant for all measurements. Material samples were evaluated in the flow cell in a sequential manner, with a rinsing step of passing LFP-free electrolyte through the cell preceding each new suspension measurement. To investigate the effect of active material loading in greater detail, LFP suspensions with different volumetric loadings were characterized in succession in a high throughput manner with the electrochemical flow cell (as an example LFP-1 is shown in Fig. 5a). The DPR values decreased as LFP loadings increased for all LFP materials, and rate of decrease of DPR with increasing loading decreased as the loading increased. Both observations were consistent with electrochemical reactions of varying numbers of particles from the suspension on average in contact with the electrode [4,24,27,28]. As active material loading increased, more particles were in contact with the current collector

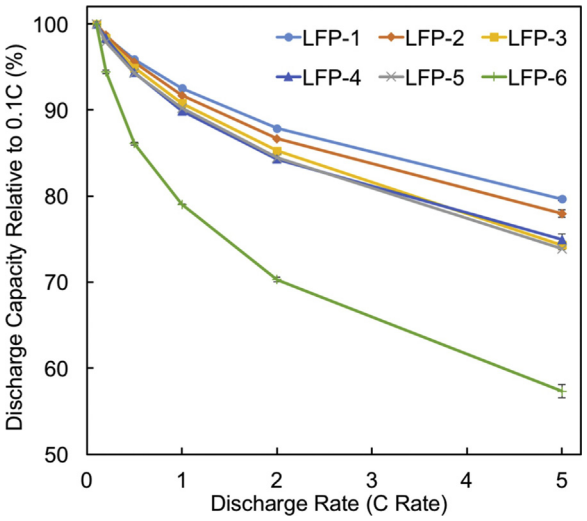

Fig. 3. Discharge capacities of all six LFP materials (light blue circle: LFP-1; orange diamond: LFP-2; yellow square: LFP-3; dark blue triangle: LFP-4; gray "x": LFP-5; green "+": LFP-6) at different C-rates relative to the capacity at 0.1C. Lines are added to guide the eye. Error Bars represent the standard deviations of three measurements for each sample (note every data point contains error bars, but that many are smaller than the data point symbols.).

electrode on average at any given time and hence were participating in electrochemical reactions and the measured oxidation currents. The particles in contact with the electrode can each be considered as resistors connected in parallel. At higher volume fractions of LFP, there were more particles on the electrode surface, resulting in more resistors in parallel and hence decreased total resistance which decreased the measured DPR. Not only was the decrease in DPR with increased loading consistent with more resistors/particles in parallel, but the proportional relationship between LFP loading and resistance also supports this analysis. If resistance from a single particle in contact with the current collector was R_i, then the collective resistance of N particle resistors in parallel (R_N) can be calculated with Eq. (1). If we assume the random sampling of the ensemble of particles in the dispersion to be relatively consistent, a representative resistance for each particle from a given LFP sample can be defined as R_0. This assumption should be reasonable because the number of particles was large even at low loadings and for a large batch of LFP sample there was not any particle sorting or separation to bias any particular dispersion. Using the assumption of a representative single resistance for each LFP sample, R_N would be R_0/N. Thus, the resistance due to the active materials, which dominates DPR measurements, would be expected to be inversely related with the number of active material particles in contact with the current collector and hence inversely related with the volumetric active material loading – at least at relatively low loadings of active material where the current collector surface was readily accessible. The inverse relationship between volumetric active material loading and DPR was supported by a least squares fit of the DPR measurements as collected at increasing loadings shown in Fig. 5a. DPR was inversely related with the LFP loading and the R^2 value of 0.992 indicates that the inverse relationship was a good fit of the collected data. The inverse relationship between DPR and volumetric particle loading provided further evidence that DPR measured the collective resistance of the active material particles. The inverse relationship between volumetric loading and DPR was analogous to previously reported experiments of the relationship between active material loading and area specific impedance in coin cells [45,46]. In both cases, the increase in particles participating in electrochemical reactions decreased the total cell resistance with an inverse relationship between particle loading and total measured resistance. Volumetric loading of 2 vol% LFP was chosen for further comparison between LFP materials because 1) the change in resistance above 2 vol% was relatively small, 2) higher loadings required more material and as an analytical technique smaller sample size was desirable, and 3) at very low loadings of LFP in some cases the variation in the measured resistance was relatively high, likely because at lower loadings the DPR measurement became more stochastic which resulted in more significant swings in the distribution of particles on the current collector relative to the mean distribution.

$$R_N = \frac{1}{\sum_{i=1}^{N} \frac{1}{R_i}} \quad (1)$$

Lower DPR for a given material indicated that material should have a slower increase of overpotential at increasing current, and thus for appropriate materials processed into equivalent electrodes and battery cells, a material with a lower DPR would in general be expected to correlate to a higher voltage and better capacity retention at increasing currents [7,24]. Thus, for a given set of materials those with lower DPR values would be expected to have better rate capability. We also note that DPR on LFP was a single measurement of multiple resistances, but was expected to be dominated by the ionic or electronic resistance of the active

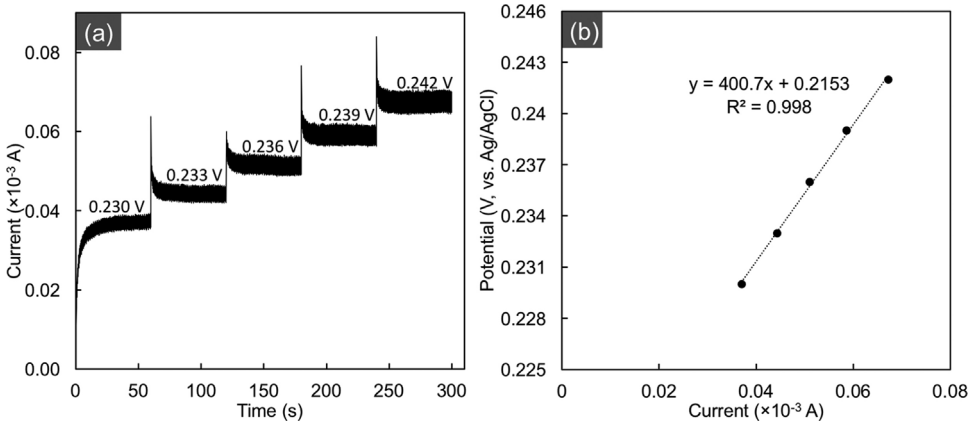

Fig. 4. Example DPR measurement for 2 vol% LFP-3 dispersed in aqueous electrolyte. (a) Chronoamperometry tests from 0.230 V to 0.242 V (vs. Ag/AgCl reference electrode) and (b) the extracted potential vs. current data set from (a). The dashed line is a linear fit with the slope, intercept, and R^2 for the fit provided in the plot area.

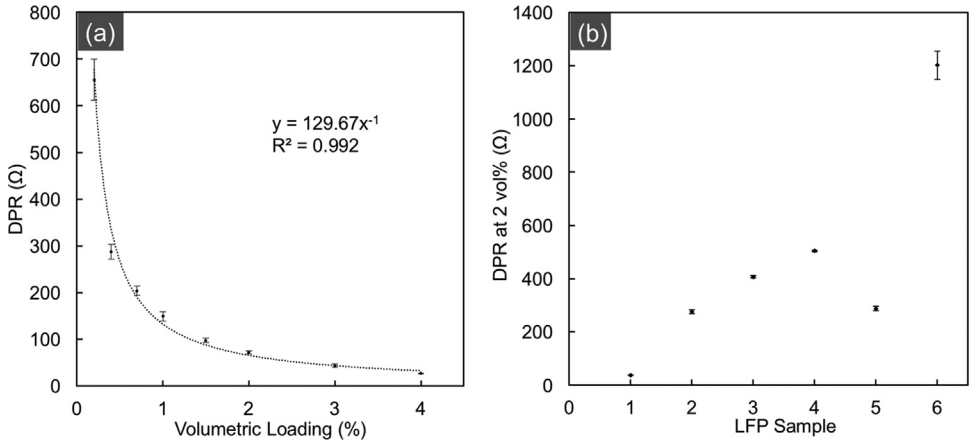

Fig. 5. (a) DPR of LFP-1 at different volumetric loadings from 0.2 vol% to 4 vol%. Dashed line was the resulting power law fit, with the resulting equation and R^2 value displayed in the plot area. (b) DPR of all six LFP materials measured at 2 vol% LFP. Bars represent the standard deviations of three measurements for each sample.

material particles. The total resistance in conventional electrodes is more complex and highly dependent on the fabrication process – though importantly DPR has the advantage of reducing the system complexity to identify what fraction of a cell resistance may be due to the active material. DPRs for all six LFP materials at 2 vol% were measured and the results are shown in Fig. 5b. Recall that the materials were numbered in order of decreasing rate capability where LFP-1 had the highest rate capability and LFP-6 had the lowest rate capability in identically processed and assembled coin cells. With the exception of LFP-5, the DPR showed an increasing trend from LFP-1 to LFP-6, with LFP-1 having the lowest DPR and LFP-6 having the highest DPR. This DPR trend was generally consistent with expectations based on the relative rate capability order of these LFP materials, where the material with the lowest DPR had the highest rate capability and the material with the highest DPR had the lowest rate capability. The standard deviations were also very small relative to the measured DPR values, indicating good data consistency. We note that the DPR values were consistent for successive measurements of the same material over the measurement timescales of less than half an hour, and thus aging effects of the electrolyte (discussed in more detail later) did not impact the relative DPR measurements in Fig. 5. LFP-5 was the outlier in the DPR analysis with regards to the correlation to relative rate capability. We speculate that this deviation was due to the significantly higher carbon loading of 3.3 wt% (from TGA measurements, TGA results for all LFP materials can be found in Fig. S3 in the Supplementary Materials), compared to 0–2 wt% for the other LFP materials. This large amount of carbon additive likely decreased the DPR due to the formation of a conductive network within local particle aggregates within the suspension that effectively increased the number of particles in contact with the current collector via the carbon network and reduced the overall resistance [47,48]. We note that relative to other studies that investigated flowing cathode materials with carbon, such as semisolid flow cells [48], the loading of active material in this study was relatively low (compare 2 vol% to >20 vol%). Thus, the carbon in the DPR measurements would impact DPR via local carbon/LFP aggregates as opposed to a viscous slurry with interconnected carbon particles throughout. Future research in our lab will aim to validate this carbon aggregate hypothesis. The additional carbon in the LFP powder, however, was not as effective in improving the rate capability in coin cell measurements because an additional 20 wt% carbon was added to each LFP electrode. The relatively high 20 wt% carbon was originally chosen to minimize the contact and matrix resistance in the electrode such that the electrochemical performance was primarily limited by the resistance from the LFP active materials. To further demonstrate the impact of the high carbon in the LFP-5 material, coin cells were fabricated without any added carbon (composite electrode contained only active material and binder) and these electrodes were cycled in coin cells (for cycling profiles see Fig. S4 in the Supplementary Materials). LFP-5 had better electrochemical performance than both LFP-3 and LFP-4 (two materials that had better rate capability than LFP-5 in electrodes with additional conductive additive, see Figs. 2 and 3) with regards to capacity at 0.1C, further confirming the influence of excess carbon for LFP-5 impacting electrochemical analysis that does not have excess carbon to mitigate this effect. The results above demonstrate that DPR can provide relative rate capabilities for materials with similar physical properties. Outlier materials can also be identified when DPR analysis was combined with other techniques such as TGA.

3.3. DPR Sensitivity to LFP Aged in Electrolyte

As an example to demonstrate the sensitivity of the DPR technique, measurements were made on the same LFP material both pristine and after aging in the electrolyte. LFP has previously

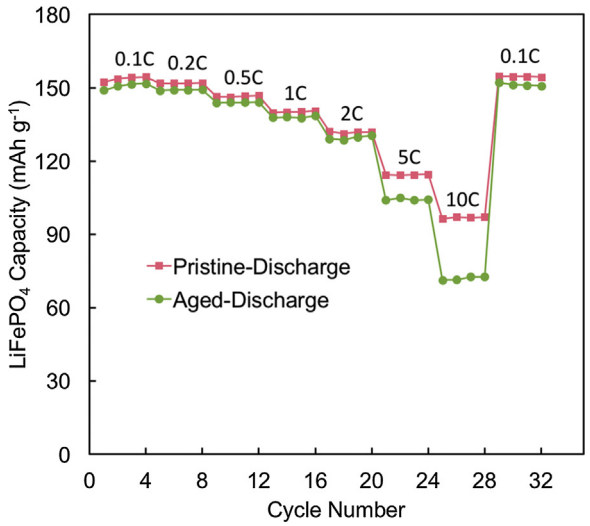

Fig. 6. Representative coin cell discharge capacity at different rates (0.1C to 10C) for pristine LFP-3 (red squares) and LFP-3 aged in 1 M Li_2SO_4 electrolyte for 15 days (green circles). Lines are added between data points to guide the eye.

been reported to have reduced electrochemical performance after being aged in water or aqueous electrolyte [13,49–52]. After aging, measured impacts to LFP include increased electrode polarization, decreased capacity, dissolution of chemical species, and in some cases a change in the crystalline phases observed in the material [13,49–52]. These performance decays can even occur during storage in humid environments, thus the storage history of LFP materials can be very important [53]. LFP changes due to contact with water in many cases proceeded slowly, and detecting these changes can be challenging without fabricating electrodes with the LFP material and performing electrochemical evaluation. As mentioned in Section 1, this procedure is very time consuming, though accurate. DPR could be a potential candidate for fast detection of the electrochemical performance decay of LFP.

As an initial demonstration of the concept of detecting LFP aging using DPR, LFP-3 was mixed with 1 M Li_2SO_4 electrolyte and aged for 15 days. After aging, the LFP was rinsed, dried, and then fabricated into electrodes and evaluated in conventional coin cells via identical procedures for the LFP batteries described earlier. A representative example of LFP-3 coin cell discharge capacity at different cycling rates, using LFP-3 material both before and after aging in electrolyte for 15 days is shown in Fig. 6. ICP measurements on the electrolyte confirmed that ~0.2% of the Fe present in the LFP had dissolved after 15 days (with total Fe concentration in the electrolyte 1 mM). While the discharge capacity at low discharge rates only dropped ~1% after aging, the high rate capacity retention dropped significantly. Relative to unaged LFP-3, the aged LFP-3 was only able to achieve ~93% of the capacity at 5C and ~80% of the capacity at 10C. This performance impact was consistent with other reports on aged LFP materials in aqueous electrolyte or water [13,49–52]. DPR tests were also conducted for both unaged and aged LFP-3 at a loading of 2 vol%. The aged LFP had a 30% increase of DPR from the unaged material (from 467.8 Ω to 626.1 Ω). This 10-minute DPR measurement detected a significant change in the aged material, indicating that DPR has the sensitivity to detect aging effects in LFP that can dramatically impact rate capability. We note that the aged LFP did not have any significant changes in the XRD pattern relative to the pristine material (see Supplemental Materials, Fig. S1) and that the DPR analysis required a timescale three orders of magnitude less than the coin cell validation of the aging impact on rate capability.

The DPR measurements described above were able to identify variations in relative rate capability between different materials and changes to the rate capability of a material due to aging. These rate capability changes, and corresponding DPR resistances, reflect the resistance of the active material particles during electrochemical oxidation. According to previous reports in the literature [7,20,23,54], the total resistance due to the LFP active material will be dependent on the ionic and/or electronic conductivity of the particles, the size of the particles, and the number of particles contributing to the electrochemical reactions. Thus, if the particle size distribution of the LFP particles is determined from another technique, DPR could be used to determine the initial conductivity of LFP particles. However, this analysis requires independent measurement of the number of particles participating in electrochemical reactions, which currently is challenging but will be a research direction for future studies. We also note that LFP was an ideal cathode candidate for this initial aqueous DPR demonstration. In addition to LFP having a charge/discharge potential within the stability window of water, LFP is also a relatively stable cathode material in water. Many other cathode materials, for example layered transition metal oxides [55], have been reported to undergo major structural changes and reductions in electrochemical performance when exposed to water. Aqueous DPR would be very challenging with these materials; although we note that the speed of the DPR technique may still allow comparative analysis between cathode materials and in particular might be suitable to determine the ability of coatings on such materials to suppress water sensitivity. If necessary and desired, DPR can also be performed with organic electrolytes for materials not suitable for aqueous suspensions [24].

4. Conclusions

LFP cathode materials were characterized electrochemically via a measured resistance during oxidation of flowing aqueous dispersions containing LFP particles. This resistance, referred to as DPR, generally was an indicator of rate capability for coin cells fabricated using the active materials. The only outlier in the analysis was a LFP sample with much higher carbon loading, further demonstrating the sensitivity of DPR to conductivity and the need for other techniques to complement analysis of the particles. DPR measurements on suspensions of systematically increasing volume fractions of LFP particles demonstrated an inverse relationship between DPR and particle concentrations. This inverse relationship was consistent with previous measurements done on coin cells with increasing active material loading within composite electrodes, indicating that the particle loading relationship to resistance in the dispersions was analogous to each additional particle in contact with the electrode representing an additional resistor connected in parallel. Sensitivity of the DPR technique was additionally used to identify changes in LFP electrochemical performance during aging in aqueous electrolyte. DPR provided a fast and sensitive approach to detect relative differences in electrochemical performance for LFP active materials, and this analysis technique should be extendable to other battery electrode materials.

Acknowledgement

This research was supported by the National Science Foundation through award ECCS-1405134. We thank Professor Geoff Geise for use of his lab's TGA instrument.

Appendix A. Supplementary data

Supplementary data associated with this article can be found, in the online version, at http://dx.doi.org/10.1016/j.electacta.2017.09.031.

References

[1] A. Vu, A. Stein, Lithium iron phosphate spheres as cathode materials for high power lithium ion batteries, J. Power Sources 245 (2014) 48–58.
[2] J. Axsen, K.S. Kurani, A. Burke, Are batteries ready for plug-in hybrid buyers? Transport Policy 17 (2010) 173–182.
[3] W.J. Zhang, Structure and performance of LiFePO4 cathode materials: A review, J. Power Sources 196 (2011) 2962–2970.
[4] Z. Qi, G.M. Koenig, Review Article Flow battery systems with solid electroactive materials, Journal of Vacuum Science & Technology B, Nanotechnology and Microelectronics: Materials, Processing, Measurement and Phenomena 35 (2017) 040801.
[5] B. Liang, Y. Liu, Y. Xu, Silicon-based materials as high capacity anodes for next generation lithium ion batteries, J. Power Sources 267 (2014) 469–490.
[6] Y. Li, S. Meyer, J. Lim, S.C. Lee, W.E. Gent, S. Marchesini, H. Krishnan, T. Tyliszczak, D. Shapiro, A.L. Kilcoyne, W.C. Chueh, Effects of Particle Size, Electronic Connectivity, and Incoherent Nanoscale Domains on the Sequence of Lithiation in LiFePO4 Porous Electrodes, Adv. Mater. (Weinheim, Ger.) 27 (2015) 6591–6597.
[7] M. Gaberscek, R. Dominko, J. Jamnik, Is small particle size more important than carbon coating? An example study on LiFePO4 cathodes, Electrochem Commun 9 (2007) 2778–2783.
[8] C. Miao, P. Bai, Q. Jiang, S. Sun, X. Wang, A novel synthesis and characterization of LiFePO4 and LiFePO4/C as a cathode material for lithium-ion battery, J. Power Sources 246 (2014) 232–238.
[9] F. Yu, S.H. Lim, Y. Zhen, Y. An, J. Lin, Optimized electrochemical performance of three-dimensional porous LiFePO4/C microspheres via microwave irradiation assisted synthesis, J. Power Sources 271 (2014) 223–230.

[10] Z. Chen, B. Du, M. Xu, H. Zhu, L. Li, W. Wang, Polyacene coated carbon/LiFePO4 cathode for Li ion batteries: Understanding the stabilized double coating structure and enhanced lithium ion diffusion kinetics, Electrochim Acta 109 (2013) 262–268.
[11] S. Wang, H. Yang, L. Feng, S. Sun, J. Guo, Y. Yang, H. Wei, A simple and inexpensive synthesis route for LiFePO4/C nanoparticles by co-precipitation, J. Power Sources 233 (2013) 43–46.
[12] J. Wang, J. Yang, Y. Tang, J. Liu, Y. Zhang, G. Liang, M. Gauthier, Y.C. Chen-Wiegart, M. Norouzi Banis, X. Li, R. Li, J. Wang, T.K. Sham, X. Sun, Size-dependent surface phase change of lithium iron phosphate during carbon coating, Nature communications 5 (2014) 3415.
[13] K. Zhong, Y. Cui, X.-D. Xia, J.-J. Xue, P. Liu, Y.-X. Tong, Study on the stability of the LiFePO4 Li-ion battery via an electrochemical method, J. Power Sources 250 (2014) 296–305.
[14] Y.-J. Lva, Y.-F. Longa, J. Sua, X.-Y. Lvb, Y.-X. Wen, Synthesis of bowl-like mesoporous LiFePO4/C composites as cathode materials for lithium ion batteries, Electrochim Acta 119 (2014) 155–163.
[15] A. Yamada, S.C. Chung, K. Hinokuma, Optimized LiFePO4 for lithium battery cathodes, J. Electrochem. Soc. 148 (2001) A224–A229.
[16] X.M. Lou, Y.X. Zhang, Synthesis of LiFePO4/C cathode materials with both high-rate capability and high tap density for lithium-ion batteries, J. Mater. Chem. 21 (2011) 4156–4160.
[17] W. Wang, B. Jiang, W. Xiong, Z. Wang, S. Jiao, A nanoparticle Mg-doped Li4Ti5O12 for high rate lithium-ion batteries, Electrochim Acta 114 (2013) 198–204.
[18] J. Liu, K. Song, P.A. van Aken, J. Maier, Y. Yu, Self-supported Li4Ti5O12-C nanotube arrays as high-rate and long-life anode materials for flexible Li-ion batteries, Nano Lett 14 (2014) 2597–2603.
[19] Z. Qi, G.M. Koenig Jr., High-Performance LiCoO2 Sub-Micrometer Materials from Scalable Microparticle Template Processing, ChemistrySelect 1 (2016) 3992–3999.
[20] M. Gaberscek, J. Jamnik, Impact of electrochemical wiring topology on the kinetics of insertion electrodes, Solid State Ionics 177 (2006) 2647–2651.
[21] F.-Y. Tsai, J.-H. Jhang, H.-W. Hsieh, C.-C. Li, Dispersion, agglomeration, and gelation of LiFePO4 in water-based slurry, J. Power Sources 310 (2016) 47–53.
[22] G. Inoue, M. Kawase, Numerical and experimental evaluation of the relationship between porous electrode structure and effective conductivity of ions and electrons in lithium-ion batteries, J. Power Sources 342 (2017) 476–488.
[23] J.-M. Atebamba, J. Moskon, S. Pejovnik, M. Gaberscek, On the Interpretation of Measured Impedance Spectra of Insertion Cathodes for Lithium-Ion Batteries, J Electrochem Soc 157 (2010) A1218.
[24] Z. Qi, G.M. Koenig Jr., Electrochemical Evaluation of Suspensions of Lithium-Ion Battery Active Materials as an Indicator of Rate Capability, J Electrochem Soc 164 (2017) A151–A155.
[25] X.L. Ji, D.Y. Liu, D.G. Prendiville, Y.C. Zhang, X.N. Liu, G.D. Stucky, Spatially heterogeneous carbon-fiber papers as surface dendrite-free current collectors for lithium deposition, Nano Today 7 (2012) 10–20.
[26] A. Zhamu, G.R. Chen, C.G. Liu, D. Neff, Q. Fang, Z.N. Yu, W. Xiong, Y.B. Wang, X.Q. Wang, B.Z. Jang, Reviving rechargeable lithium metal batteries: enabling next-generation high-energy and high-power cells, Energ Environ Sci 5 (2012) 5701–5707.
[27] Z. Qi, G.M. Koenig, A carbon-free lithium-ion solid dispersion redox couple with low viscosity for redox flow batteries, J. Power Sources 323 (2016) 97–106.
[28] Z. Qi, A.L. Liu, G.M. Koenig Jr., Carbon-free Solid Dispersion LiCoO2 Redox Couple Characterization and Electrochemical Evaluation for All Solid Dispersion Redox Flow Batteries, Electrochim Acta 228 (2017) 91–99.
[29] T. Liu, L. Zhao, D. Wang, J. Zhu, B. Wang, C. Guo, Carbon-coated single-crystalline LiFePO4 nanocomposites for high-power Li-ion batteries: the impact of minimization of the precursor particle size, RSC Adv 4 (2014) 9.
[30] J.L. Li, B.L. Armstrong, J. Kiggans, C. Daniel, D.L. Wood, Lithium Ion Cell Performance Enhancement Using Aqueous LiFePO4 Cathode Dispersions and Polyethyleneimine Dispersant, J Electrochem Soc 160 (2013) A201–A206.
[31] K. Xu, Electrolytes and Interphases in Li-Ion Batteries and Beyond, Chem. Rev. (Washington, DC, U . S.) (2014) 11503–11618.
[32] E. Quartarone, P. Mustarelli, Electrolytes for solid-state lithium rechargeable batteries: recent advances and perspectives, Chem Soc Rev 40 (2011) 2525–2540.
[33] M. Shieber, J. Inorg. Nucl. Chem 26 (1964) 1363.
[34] Fisher, Am. Mineral. 43 (1958) 761.
[35] A. Eftekhari, LiFePO4/C nanocomposites for lithium-ion batteries, J. Power Sources 343 (2017) 395–411.
[36] J.-K. Kim, D.-S. Kim, D.-H. Lim, A. Matic, G.S. Chauhan, J.-H. Ahn, Effect of carbon coating methods on structural characteristics and electrochemical properties of carbon-coated lithiumiron phosphate, Solid State Ionics 262 (2014) 25–29.
[37] V. Srinivasan, J. Newman, Design and optimization of a natural graphite/iron phosphate lithium-ion cell, J Electrochem Soc 151 (2004) A1530–A1538.
[38] K.N. Wood, M. Noked, N.P. Dasgupta, Lithium Metal Anodes: Toward an Improved Understanding of Coupled Morphological, Electrochemical, and Mechanical Behavior, ACS Energy Lett 2 (2017) 664–672.
[39] K.-H. Chen, K.N. Wood, E. Kazyak, W.S. LePage, A.L. Davis, A.J. Sanchez, N.P. Dasgupta, Dead lithium: mass transport effects on voltage, capacity, and failure of lithium metal anodes, J. Mater. Chem. A 5 (2017) 11671–11681.
[40] R. Ruffo, F. La Mantia, C. Wessells, R.A. Huggins, Y. Cui, Electrochemical characterization of LiCoO2 as rechargeable electrode in aqueous LiNO3 electrolyte, Solid State Ionics 192 (2011) 289–292.
[41] S.S. Zhang, T.R. Jow, Aluminum corrosion in electrolyte of Li-ion battery, J. Power Sources (2002) 458–464.
[42] C. Honda, S. Kikuchi, T. Ito, S. Onodera, A. Nagai, T. Ito, K. Tachibana, T. Nishina, Evaluation of Contact Resistance of Aluminum Current Collector Surfaces for Energy Storage Systems, Electrochemistry 82 (2014) 328–330.
[43] X. Zhang, T.M. Devine, Identity of Passive Film Formed on Aluminum in Li-Ion Battery Electrolytes with LiPF[sub 6], J Electrochem Soc 153 (2006) B344–B351.
[44] B. Markovsky, F. Amalraj, H.E. Gottlieb, Y. Gofer, S.K. Martha, D. Aurbach, On the Electrochemical Behavior of Aluminum Electrodes in Nonaqueous Electrolyte Solutions of Lithium Salts, J Electrochem Soc 157 (2010) A423–A429.
[45] K.G. Gallagher, P.A. Nelson, D.W. Dees, Simplified calculation of the area specific impedance for battery design, J. Power Sources 196 (2011) 2289–2297.
[46] D. Dees, E. Gunen, D. Abraham, A. Jansen, J. Prakash, Electrochemical Modeling of Lithium-Ion Positive Electrodes during Hybrid Pulse Power Characterization Tests, J Electrochem Soc 155 (2008) A603–A613.
[47] Z. Li, K.C. Smith, Y.J. Dong, N. Baram, F.Y. Fan, J. Xie, P. Limthongkul, W.C. Carter, Y.M. Chiang, Aqueous semi-solid flow cell: demonstration and analysis, Phys Chem Chem Phys 15 (2013) 15833–15839.
[48] M. Duduta, B. Ho, V.C. Wood, P. Limthongkul, V.E. Brunini, W.C. Carter, Y.M. Chiang, Semi-Solid Lithium Rechargeable Flow Battery, Adv. Energy Mater. 1 (2011) 511–516.
[49] P. Liu, J. Wang, J. Hicks-Garner, E. Sherman, S. Soukiazian, M. Verbrugge, H. Tataria, J. Musser, P. Finamore, Aging Mechanisms of LiFePO[sub 4] Batteries Deduced by Electrochemical and Structural Analyses, J Electrochem Soc 157 (2010) A499.
[50] Y. Yin, Y.-h. Wen, Y.-l. Lu, J. Cheng, G.-p. Cao, Y.-s. Yang, Electrochemical Performance and Capacity Fading Mechanism of LiFePO4 at Different pH Aqueous Electrolyte Solutions, Chinese J Chem Phys 28 (2015) 315–322.
[51] M. Koltypin, D. Aurbach, L. Nazar, B. Ellis, On the Stability of LiFePO[sub 4] Olivine Cathodes under Various Conditions (Electrolyte Solutions, Temperatures), Electrochem Solid St 10 (2007) A40.
[52] W. Porcher, P. Moreau, B. Lestriez, S. Jouanneau, F. Le Cras, D. Guyomard, Stability of LiFePO4 in water and consequence on the Li battery behaviour, Ionics 14 (2008) 583–587.
[53] N. Iltchev, Y. Chen, S. Okada, J.-i. Yamaki, LiFePO4 storage at room and elevated temperatures, J. Power Sources 119-121 (2003) 749–754.
[54] M. Gaberscek, A Method for Fast Estimation of the Rate-Limiting Step in Lithium-Ion Batteries, Acta Chim Slov 61 (2014) 480–487.
[55] Z. Chen, J. Wang, J. Huang, T. Fu, G. Sun, S. Lai, R. Zhou, K. Li, J. Zhao, The high-temperature and high-humidity storage behaviors and electrochemical degradation mechanism of LiNi 0.6 Co 0.2 Mn 0.2 O 2 cathode material for lithium ion batteries, J. Power Sources 363 (2017) 168–176.